Dead Reckoning Navigation with IMU and Magnetometer

Lab 4 Report

EECE5554: Robotics Sensing and Navigation

Group 4:

Wondmgezahu Teshome (me)
Kanishk Kaushal
Matthew Kazan
Sam Milhaven (driver code)

April 9, 2025

1 Introduction

Dead reckoning navigation represents a fundamental technique in autonomous vehicle systems, enabling position tracking when GPS signals are unavailable or unreliable. This lab investigates the integration of Inertial Measurement Unit (IMU) data for position estimation through dead reckoning, and compares its performance against GPS ground truth. The VectorNav VN-100 IMU combines three-axis accelerometers, gyroscopes, and magnetometers to provide comprehensive motion data. While GPS offers absolute positioning with bounded error, IMU-based dead reckoning provides high-frequency updates but suffers from integration drift over time. This lab explores magnetometer calibration, sensor fusion techniques for heading estimation, velocity determination through acceleration integration, and ultimately full trajectory reconstruction.

2 Data Collection

For this experiment, we utilized two primary sensors: the VectorNav VN-100 IMU configured to output data through a custom ROS2 driver, and a GPS puck providing reference position data. The IMU driver parsed the VNYMR string containing acceleration, angular velocity, orientation, and magnetometer readings. The data collection was conducted in two phases using the NUANCE autonomous vehicle:

Magnetometer Calibration Data: A calibration dataset was collected near Ruggles station square, driving in circles 4-5 times to capture the full rotation of the vehicle. This pattern is optimal for identifying hard-iron and soft-iron effects affecting the magnetometer.

Navigation Dataset: Following calibration, we drove the vehicle on a loop around Boston. The route included at least 10 turns. Both sensors were connected to a single laptop running ROS2, with data captured in rosbag format for subsequent analysis. Throughout the collection process, we continuously monitored data streams to ensure consistent recording from both sensors.

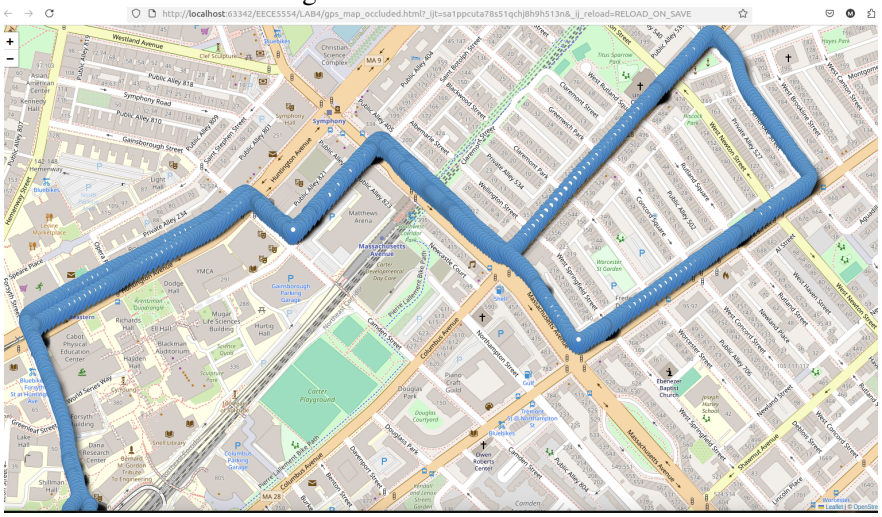

Figure 1: Navigation dataset

3 Results and Analysis

3.1 Calibration of Magnetometer

Plots:

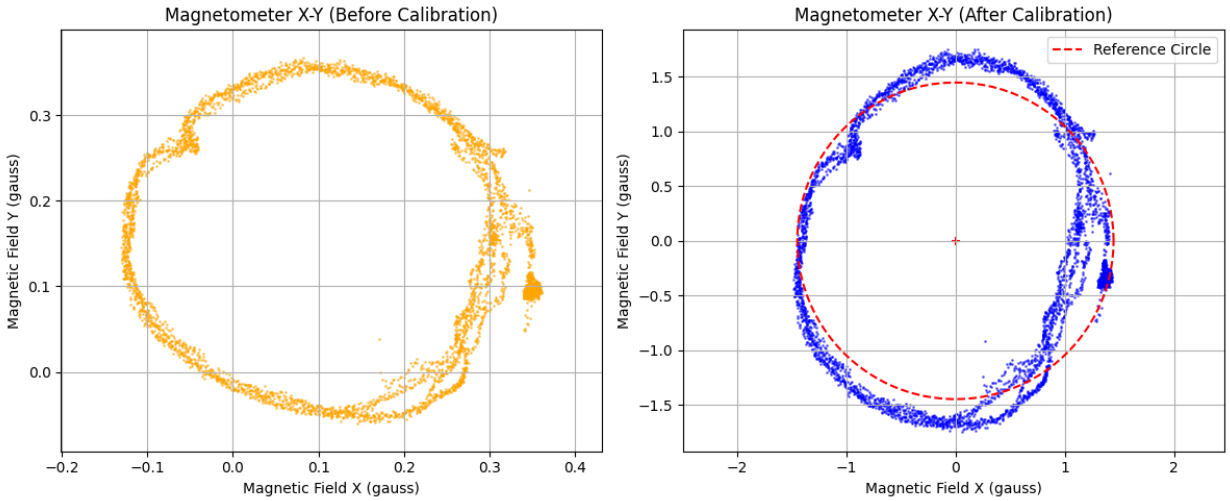

Figure 2: X-Y plots of magnetometer data before calibration (left, showing offset and distortion) and after calibration (right)

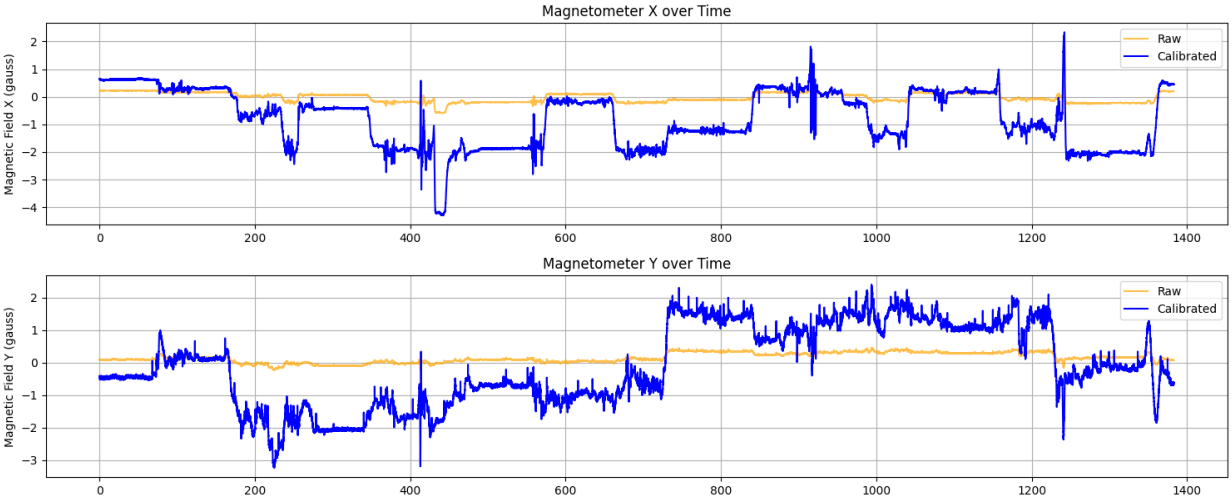

Figure 3: Time series of magnetometer X and Y readings showing raw (orange) and calibrated (blue) data, demonstrating the increased dynamic range and proper zero-centering achieved through calibration.

Discussion: The magnetometer calibration results demonstrate successful correction of both hard-iron and soft-iron effects in the sensor data. Figure 2 provides clearer visualization of the calibration effectiveness through X-Y plots. Before calibration (left plot), the data forms an offset circle centered around $X \approx 0.15$, $Y \approx 0.15$ with slight elliptical distortion, indicating both hard-iron (offset) and soft-iron (distortion) effects. After calibration (right plot), the data forms a well-centered circle at the origin with proper scaling (-1.5 to +1.5 gauss range), confirming successful correction of both effects. In Figure 3, we see time series plots showing raw magnetometer readings (orange) with minimal variation around non-zero offsets, while

the calibrated data (blue) displays properly centered readings with appropriate amplitude ranges. The raw X and Y data hover around positive values (0.1-0.3 gauss), indicating significant hard-iron bias that was effectively removed in calibration. The transformation from a small, offset ellipse to a centered, well-formed circle indicates that calibration algorithm effectively addressed the magnetic distortions present in the vehicle environment.

3.2 Yaw Estimation

Plots:

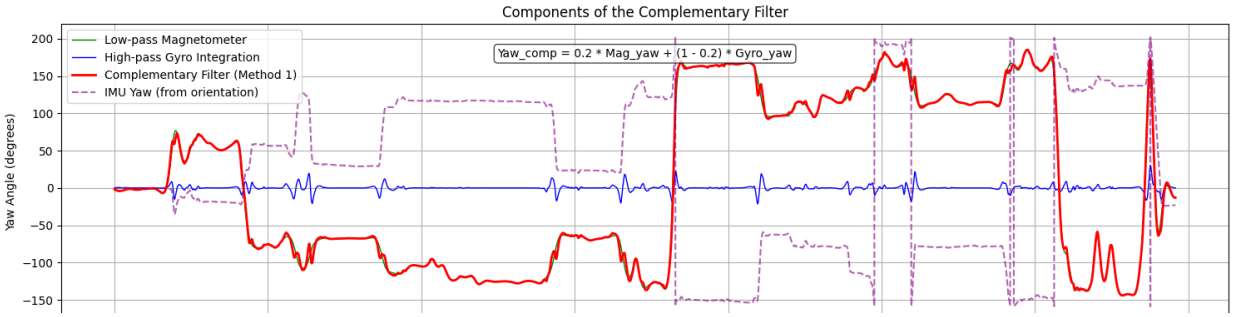

Figure 4: Components of the complementary filter showing low-pass filtered magnetometer data (green), high-pass filtered gyro integration (blue), the resulting complementary filter output (red) using a weight of 0.2 for magnetometer and 0.8 for gyro data, and the IMU's internal yaw calculation (purple dashed) for comparison.

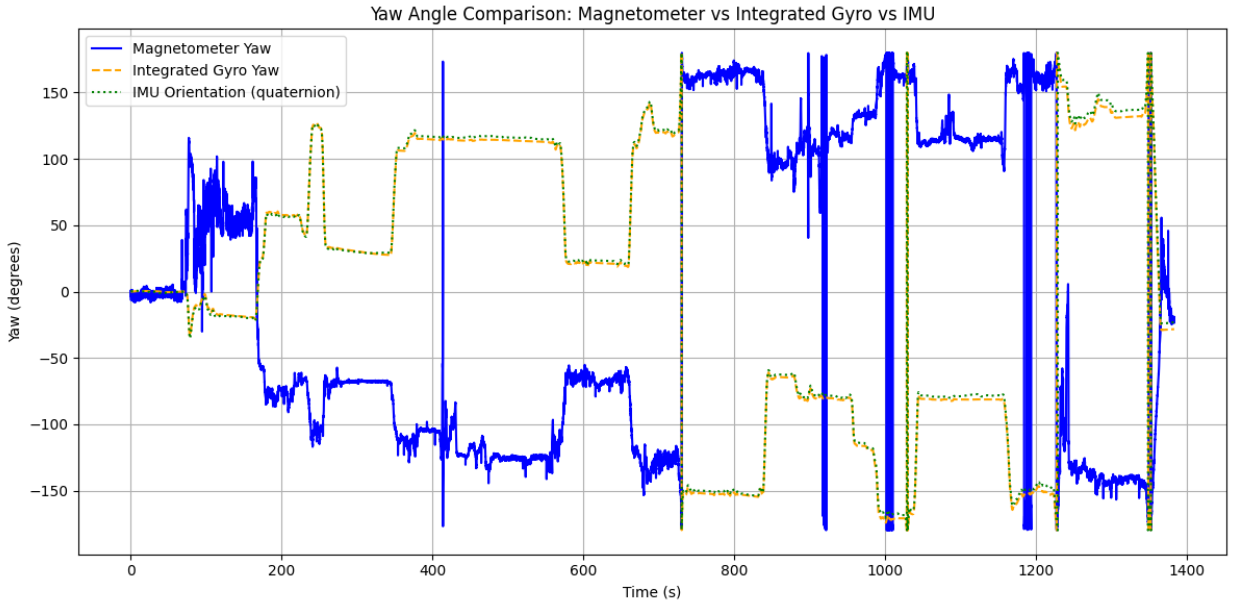

Figure 5: Comparison of yaw angle estimates from three different methods

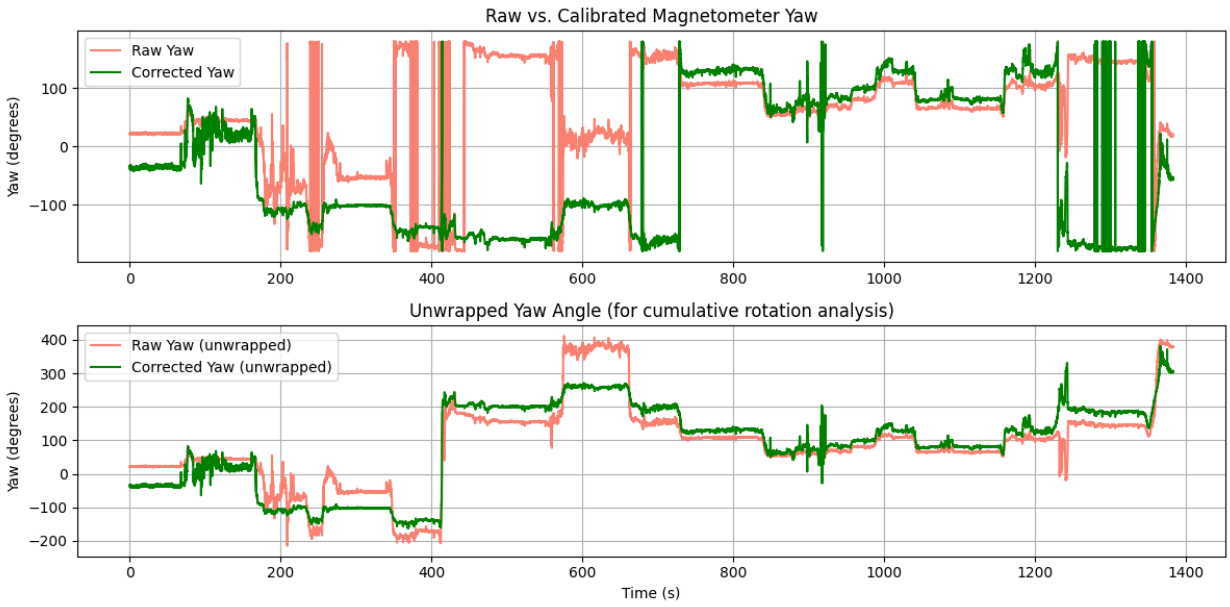

Figure 6: Comparison of magnetometer yaw angles

Discussion The implemented complementary filter effectively combines magnetometer and gyroscope data with a weight ratio of $\alpha = 0.2$ for magnetometer and (1-α)=0.8 for gyroscope measurements, applying a low-pass filter (cutoff 0.05 Hz) to magnetometer data and a high-pass filter to integrated gyro data. This approach leverages the complementary strengths of both sensors: the absolute reference but noisy measurements from the magnetometer and the smooth but drift-prone measurements from the gyroscope. In Figure 4, we can observe how the filter components contribute to the final heading estimate. The high-pass filtered gyro integration (blue) captures rapid changes with minimal noise, while the low-pass filtered magnetometer (green) provides long-term stability. Their combination (red) creates heading estimate that tracks the IMU's quaternion-based orientation (purple) closely while avoiding both gyroscope drift and magnetometer noise. Figure 5 demonstrates that the integrated gyroscope data and IMU's quaternion-based orientation show good alignment, while the magnetometer data, though noisier, captures the same general heading patterns. The agreement between these different measurement methods validates that the calibration procedure successfully corrected the magnetometer distortions. Figure 6 further confirms the effectiveness of the calibration, with the unwrapped view particularly useful for visualizing the continuous vehicle rotation history without the discontinuities that occur at 180 degree transitions. This complementary filter implementation provides an optimal yaw estimate by using the 0.2/0.8 weighting to balance between the absolute reference provided by the magnetometer and the short-term measurements from the gyroscope.

3.3 Velocity Estimation

Plots:

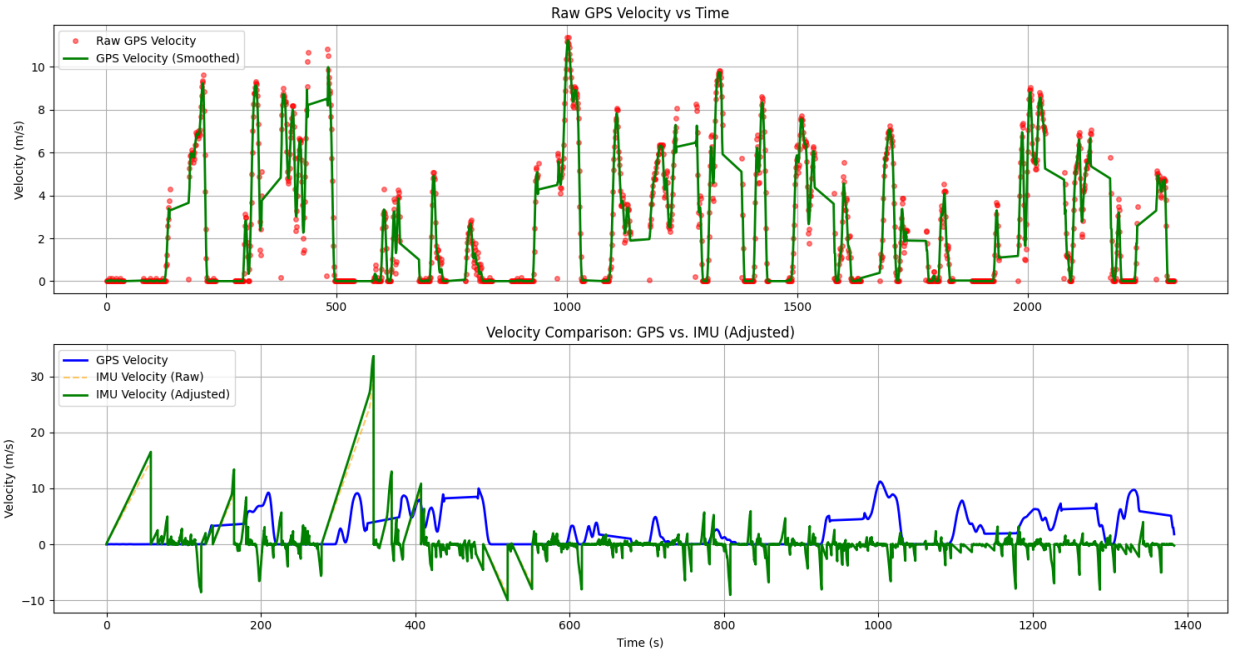

Figure 7: Velocity estimation comparison showing raw GPS velocity measurements (red points) with smoothed version (green line) in the top panel, and the comparison between GPS velocity (blue), raw IMU velocity integration (orange dashed), and adjusted IMU velocity (green) in the bottom panel.

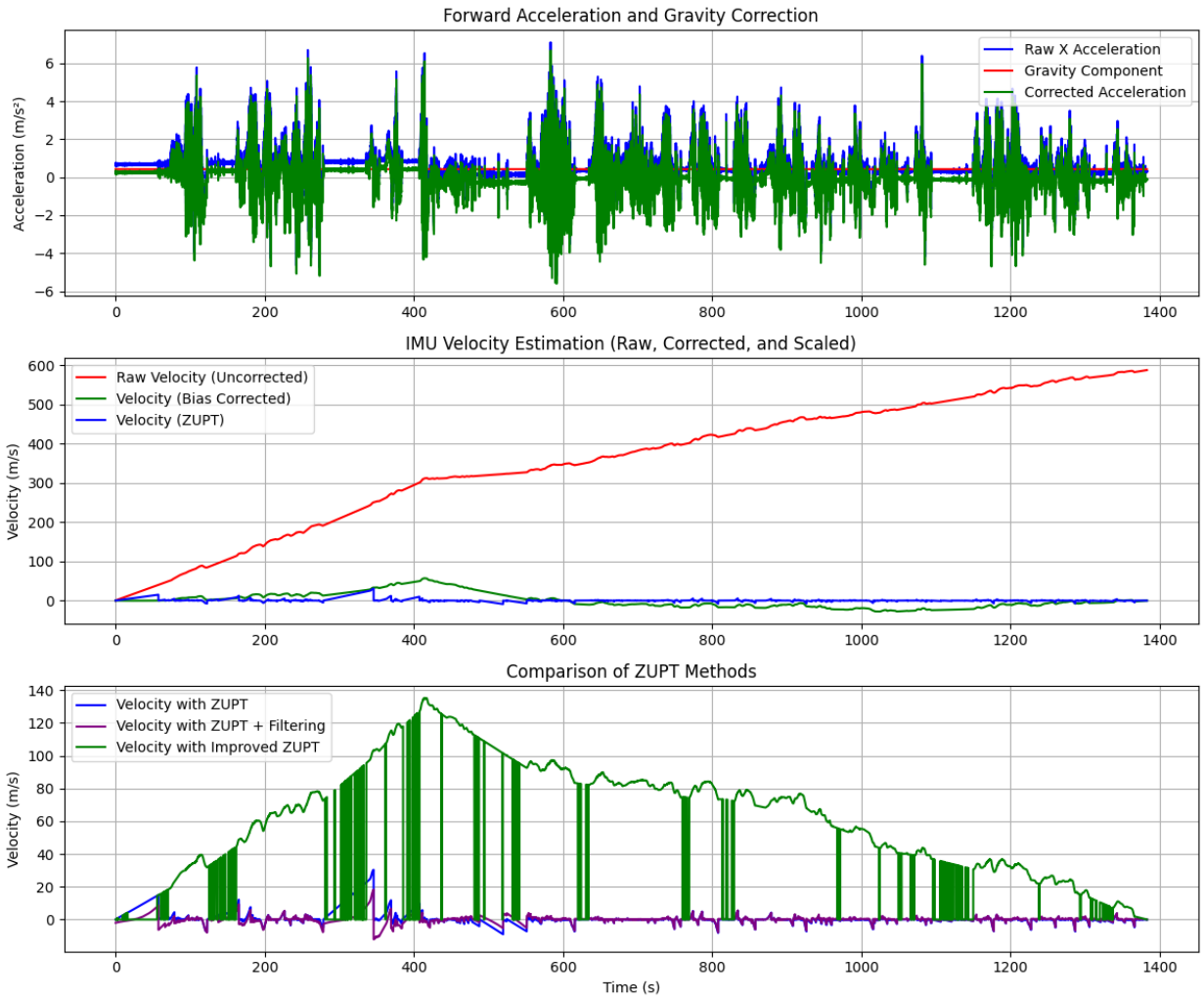

Figure 8: Acceleration processing and velocity estimation showing three stages: (top) raw acceleration data with gravity component removal, (middle) different velocity integration approaches demonstrating significant drift in the raw integration, and (bottom) comparison of three Zero Velocity Update (ZUPT) methods applied to manage integration drift.

Discussion The velocity estimation demonstrates significant challenges in using accelerometer data for dead reckoning navigation. In Figure 7, the raw GPS velocity shows the typical urban driving pattern with speeds ranging from 0-11 m/s, with clear stationary periods at traffic stops. The comparison in the bottom panel shows substantial discrepancies between the GPS and IMU velocity measurements, with the IMU data showing extreme spikes exceeding 30 m/s at certain points and poor tracking of the GPS reference after scaling. Figure 8 illustrates the progressive steps in processing accelerometer data. The top panel shows the successful removal of gravity bias from the raw acceleration (blue) by identifying the mean offset (red) to produce the corrected signal (green). The middle panel shows the drift problem in raw acceleration integration (red curve reaching 600 m/s), which is partially addressed by bias correction (green) but still not enough for practical use. The bottom panel compares three ZUPT implementations: a basic acceleration threshold method (blue), a high-pass filtered version (purple), and an alternative approach using acceler-

ation standard deviation (green) to detect stationary periods. While the simple ZUPT and filtered ZUPT methods successfully reset velocity to zero during stops, the "improved" standard deviation approach shows worse performance with unrealistic velocity values exceeding 100 m/s. This unexpected result likely stems from the challenge of selecting an appropriate standard deviation threshold that can differentiate between genuine stops and normal acceleration variations in urban driving. The implementation demonstrates why accelerometer-based velocity estimation remains problematic for extended navigation without regular position fixes, as even minor bias errors compound rapidly through integration despite the application of various ZUPT techniques.

3.4 Vehicle Motion Model

Plots:

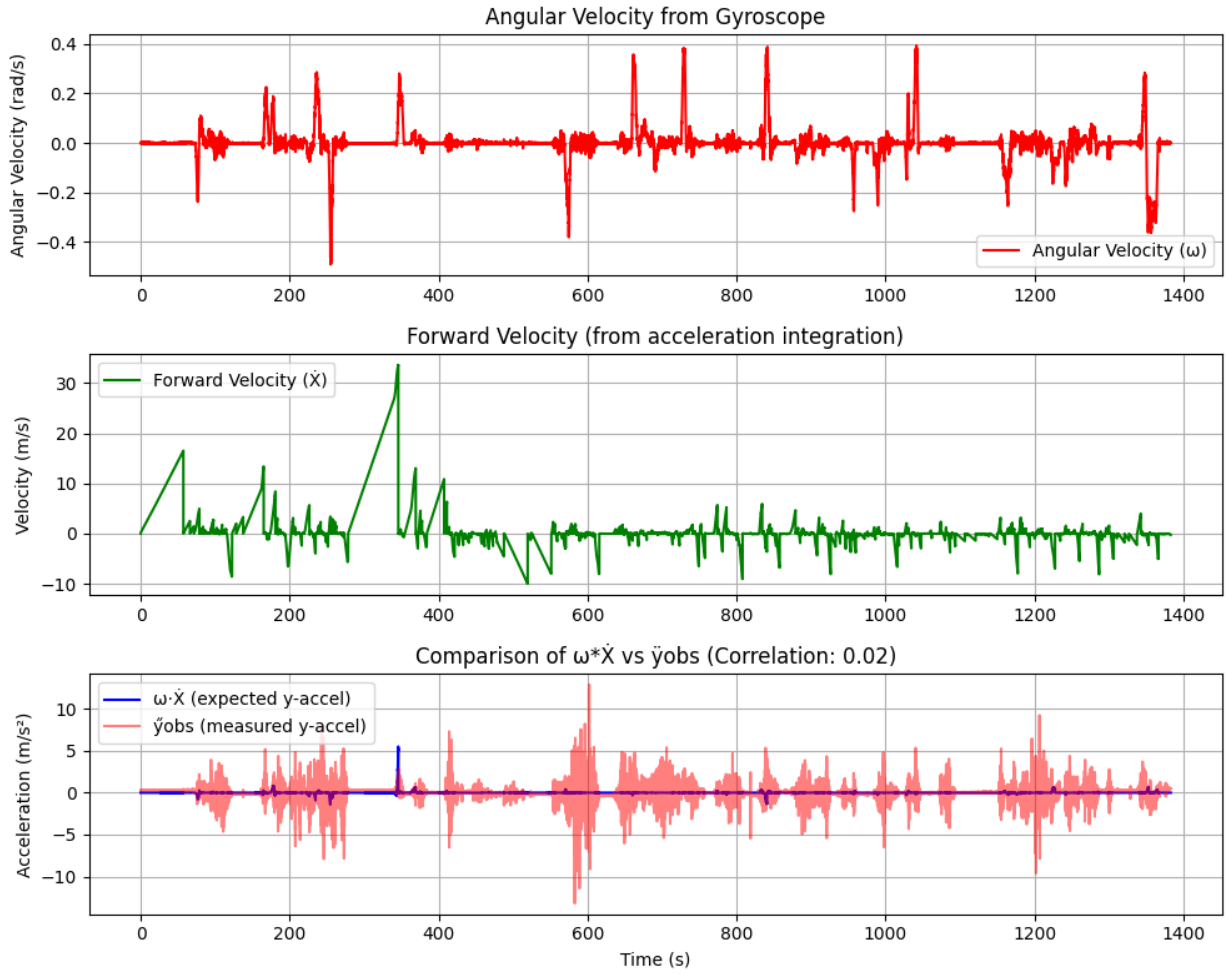

Figure 9: Vehicle motion model analysis

Discussion This figure examines the simplified vehicle motion model described in the lab instructions, which predicts that lateral acceleration (yobs) should approximately equal the product of angular velocity (ω) and forward velocity when assuming the vehicle is not skidding sideways and the IMU is mounted at the center of mass (xc = 0). The extremely low correlation coefficient (0.02) between the predicted

lateral acceleration (blue) and the measured lateral acceleration (red) indicates the simplified model fails to accurately represent the vehicle's actual dynamics in this experiment. This significant discrepancy could be attributed to several factors: the IMU was mounted with some offset from the vehicle's center of rotation (xc $\neq$ 0), or measurement noise and integration errors in the velocity estimation created compounding inaccuracies. The measured lateral acceleration shows substantially larger amplitudes (frequently reaching $\pm$5 m/s²) compared to the predicted values (sometimes exceeding $\pm$1 m/s²), suggesting the model is missing important dynamics components. This result demonstrates why more sophisticated models is necessary for accurate dead reckoning navigation in real-world driving conditions.

3.5 Trajectory Estimation with Dead Reckoning

Plots:

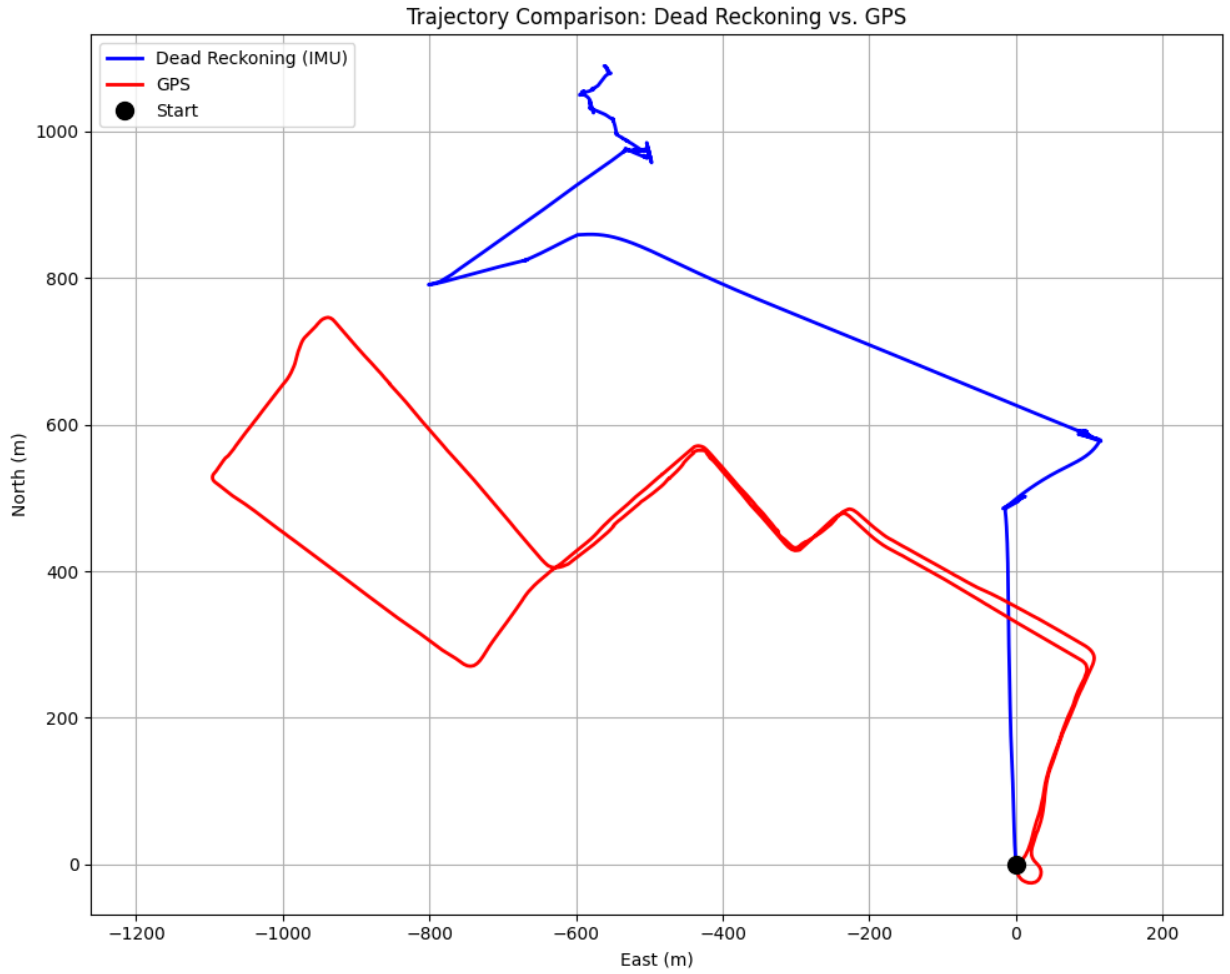

Figure 10: Comparison between the estimated trajectory from dead reckoning (blue) and GPS ground truth (red).

Figure 11: Dead reckoning position error growth over time

Discussion

The trajectory estimation results demonstrate the fundamental limitations of IMU-only dead reckoning for extended navigation. Despite the careful calibration of the magnetometer, implementation of complementary filtering for yaw estimation, and application of various ZUPT techniques for velocity estimation, the accumulated position error grows catastrophically, exceeding 400 meters within just the first 100 seconds of travel. The trajectory comparison in Figure 10 shows that while the GPS path (red) shows driving pattern with clear street grid patterns, the dead reckoning path (blue) bears almost no similarity to the actual route. The IMU-derived path diverges dramatically in both direction and scale, ultimately placing the vehicle approximately 800 meters from its true position after the 23-minute journey. This poor performance can be attributed to several factors: (1) errors in heading estimation despite complementary filtering, (2) velocity estimation challenges as seen in previous figures, (3) the simplified vehicle motion model that showed very poor correlation with actual lateral acceleration (0.02), and (4) the mathematical reality that small errors in both heading and velocity are integrated twice to yield position, causing errors to grow quadratically with time. The results also demonstrate why IMUs like the VectorNav VN-100 still require regular position fixes from absolute positioning systems like GPS. This experiment clearly illustrates why sensor fusion between complementary systems (GPS for absolute positioning and IMU for short-term dynamics) remains essential for robust vehicle navigation.

Answer to the Questions: (most of them answered in the discussion, but I put them here in short for convenience).

Q1: the magnetometer is calibrated using min/max method for hard-iron correction and eigenvalue decomposition for soft-iron effects. The hard-iron distortion (bias/offset) was evident from the off-center position of the uncalibrated data, while soft-iron distortion was visible in the elliptical rather than circular shape of the plots. These distortions potentially came from some magnetic materials in the vehicle.

Q2: Raw magnetometer readings (in gauss) were converted to yaw angles using the arctangent function: yaw = arctan2(my, mx), where my and mx are the magnetometer's y and x components. This result in radians was then converted to degrees by multiplying by $180/\pi$.
Q3:The complementary filter combined low-pass filtered magnetometer data with high-pass filtered gyroscope integration using a cutoff frequency of 0.05 Hz. The equation was: $Yaw_{comp} = 0.2 * Mag_{yaw} + (1 - 0.2) * Gyro_{yaw}$ This gives 20% weight to the magnetometer data and 80% to the gyroscope integration.
Q4: Based on the data analysis, the integrated gyro yaw and IMU quaternion-based orientation would be most trusted for navigation as they showed remarkable agreement and stability. While the complementary filter combines advantages of both sensors, our specific implementation wasn't optimized enough to outperform the IMU's internal orientation estimation for this dataset.
Q5: I applied gravity component removal, Zero Velocity Update (ZUPT) to reset velocity during stops, and scaling based on GPS velocity reference. These adjustments were necessary to combat the severe integration drift inherent in accelerometer data.
Q6: Major discrepancies included severe drift in raw accelerometer velocity (reaching 600+ m/s), inconsistent detection of stationary periods, and significant unrealistic spikes. These issues occur because accelerometer integration amplifies sensor noise, gravity effects are difficult to perfectly remove, and integration errors accumulate over time.
Q7: They show very poor agreement with a correlation of only 0.02. The measured lateral acceleration shows much larger amplitudes (± 5) than predicted by $\omega\dot{x}$ (rarely exceeding ± 1). This difference stems from vehicle skidding, IMU positioning offset from center of mass, and limitations of the simplified model.
Q8: The trajectory was estimated by integrating velocity components using $v_east = velocity_x * sin(yaw)$ and $v_{north} = velocity_x * cos(yaw)$. Despite both starting at the origin, the dead reckoning path diverges dramatically from the GPS ground truth, with errors exceeding 800 meters. No additional scaling was applied beyond the initial velocity calibration.
Q9:The VectorNav VN-100 would typically be expected to maintain reasonable accuracy for 30-60 seconds without position fixes. However, our system exceeded the 2m error threshold almost immediately (within seconds). This poor performance resulted from compounding velocity integration errors, simplified motion model assumptions not holding in real driving conditions, and the quadratic growth of positioning errors over time.

4 Conclusion

In this lab, we showed both the capabilities and limitations of IMU-based dead reckoning navigation. Magnetometer calibration successfully corrected hard-iron and soft-iron distortions, enabling more accurate heading estimation. However, velocity estimation from accelerometer data proved challenging despite implementing various Zero Velocity Update techniques, with significant drift remaining even after corrections. The vehicle motion model showed poor correlation (0.02) between predicted and measured lateral acceleration, indicating the simplified model inadequately represented real-world vehicle dynamics.And finally, the dead reckoning position error grew catastrophically, exceeding 400 meters within just 100 seconds and ulti-

mately reaching over 800 meters of deviation. These results confirm that while inertial navigation systems provide valuable short-term motion data, they cannot reliably operate independently for extended periods without absolute position references. This experiment highlights why sensor fusion between GPS and IMU remains essential for robust navigation systems in autonomous vehicles and robotics applications.